

Seasonal and interannual variabilities in tropical tropospheric ozone

J. R. Ziemke¹

Software Corporation of America, Beltsville, Maryland

S. Chandra

NASA Goddard Space Flight Center, Greenbelt, Maryland

Abstract. This paper presents the first detailed characterization of seasonal and interannual variability in tropical tropospheric column ozone (TCO) to delineate the relative importance of biomass burning and large-scale transport. TCO time series are derived from 20 years (1979–1998) of total ozone mapping spectrometer (TOMS) data using the convective cloud differential (CCD) method. Our study identifies three regions in the tropics with distinctly different characteristics related to seasonal and interannual variability. These three regions are the eastern Pacific, Atlantic, and western Pacific. TCO in the Atlantic region peaks at about the same time (September–October) both north and south of the equator, while the annual-cycle amplitude in TCO varies from about 3 to 6 Dobson units (DU) from north to south of the equator. In comparison, annual cycles in both the eastern and western Pacific are generally weak, with the largest TCO amount occurring around March–April in the northern hemisphere and September–November in the southern hemisphere. Interannual variabilities in these three regions are also very different. The Atlantic region indicates a predominant quasi-biennial oscillation (QBO) in TCO which is out of phase with the QBO in stratospheric ozone. This behavior is consistent with a UV modulation of upper tropospheric photochemistry on a QBO timescale caused by the QBO in stratospheric ozone. However, photochemical models predict significantly smaller changes, and dynamical effects may be a critical factor. Interannual variability in TCO in the Atlantic also appears to have some influence from biomass burning, but our study indicates that it is of lesser significance. Interannual variability in the eastern and western Pacific is dominated by El Niño events. During an El Niño there is anomalously low TCO in the eastern Pacific and high values in the western Pacific. These signatures indicate combined effects of convectively driven transport and tropospheric ozone generated by intense biomass burning in the Indonesian region. Finally, a simplified tropospheric ozone residual (STOR) method which utilizes the small variability of TCO near the dateline is proposed in this study to derive high-resolution maps and extended time series of TCO.

1. Introduction

It is generally recognized that the seasonal maximum in tropospheric column ozone (TCO) in the tropical South Atlantic region is related to intense biomass burning in Africa and Brazil during southern spring [Crutzen and Andreae, 1990; Fishman *et al.*, 1990, 1991, 1992; Watson *et al.*, 1990]. A number of papers published in the special issue of the *Journal of Geophysical Research*

[e.g., Fishman *et al.*, 1996; Thompson *et al.*, 1996; Krishnamurti *et al.*, 1996; Jacob *et al.*, 1996], as a part of the Transport and Atmospheric Chemistry Near the Equator–Atlantic (TRACE-A) campaign, have provided a broader understanding of the relationship between biomass burning and tropospheric ozone in the tropics. These studies suggested that the presence of biomass burning in South America and southern Africa is a primary source of ozone precursors (e.g., CO, NO_x, and hydrocarbons) which may lead to 10–15 Dobson unit (DU) increases in tropospheric column ozone in this region. Similar conclusions have also been arrived at by Wang *et al.* [1998a] and Basseur *et al.* [1998] using three-dimensional transport models.

¹Also at NASA Goddard Space Flight Center, Greenbelt, Maryland.

This paper is not subject to U.S. copyright. Published in 1999 by the American Geophysical Union.

Paper number 1999JD900277.

The interpretation of the South Atlantic anomaly in tropical ozone in terms of biomass burning is complicated by the fact that a number of meteorological parameters also show a predominant zonal wave 1 structure similar to TCO, thus raising the possibility that the anomaly may be of meteorological origin [e.g., *Krishnamurti et al.*, 1993; *Ziemke and Chandra*, 1998]. For example, the transport model used by *Krishnamurti et al.* [1993] for October months showed that tropospheric subsidence and horizontal transport of air (caused by persistent planetary-scale circulation) in the South Atlantic region can produce an ozone peak in this region even in the absence of biomass burning. In the Indonesian region the anomalous increase of 10-20 DU in TCO during the 1997-1998 El Niño [*Chandra et al.*, 1998] clearly highlights the difficulty of delineating the relative importance of dynamical and biogenic processes. During this period, there were large-scale fires in the tropical rain forests of Indonesia. There was also a major shift in the atmospheric convection pattern from the western to the eastern Pacific. As suggested by *Chandra et al.* [1998], the increase in TCO and decrease in upper tropospheric water vapor in the Indonesian region during the 1997-1998 El Niño was caused by a combination of large-scale circulation processes associated with the shift in the tropical convection pattern and the surface/boundary layer processes associated with the fires in this region.

It is apparent that to gain further insight into the relative role of photochemical and transport processes in the tropical troposphere one needs to better characterize ozone variability over a longer period in terms of perturbations associated with biomass burning, convective activity, and changes in column ozone above the tropopause. The latter affects solar UV radiation entering the troposphere and alters the photochemistry of tropospheric O₃ [e.g., *Liu and Trainer*, 1988; *Madronich*, 1993; *Fuglestedt et al.*, 1994; *Haigh*, 1996]. Because the stratosphere is strongly influenced by the solar cycle and quasi-biennial oscillation (QBO), it may also produce variability in the troposphere on these timescales through modulation of UV flux entering the troposphere. We note that *Chandra et al.* [1999] found a solar-cycle signal in TCO (~2-3 DU peak-to-peak) in the marine tropical troposphere that was out of phase with the solar cycle in stratospheric column O₃. It was found that photochemical models could not explain this phenomenon from UV modulation and that its origin may involve subtle changes in transport over the timescale of a solar cycle.

The purpose of this paper is to characterize and present plausible explanations for observed variabilities in TCO from 20 years (1979-1998) of total ozone mapping spectrometer (TOMS) data using the convective cloud differential (CCD) method [*Ziemke et al.*, 1998]. TCO time series data represent monthly mean values binned to a 5° × 5° grid. Tropical convective activity is inferred from the Southern Oscillation index (SOI)

and National Oceanic and Atmospheric Administration (NOAA) outgoing longwave radiation (OLR) data [*Liebmann and Smith*, 1996]. Biomass burning events are identified using TOMS aerosol-smoke index (ASI) measurements [*Hsu et al.*, 1996; *Herrman et al.*, 1997]. Both OLR and ASI data were also binned to a monthly 5° × 5° grid for studying the relative variability of TCO with respect to these parameters.

Our study begins with a description of data and analysis (section 2) followed by a general overview of tropospheric O₃ (section 3), and then annual cycles (section 4), interannual variability (section 5), a simplified method for deriving TCO (section 6), and finally, a summary (section 7).

2. Data and Analysis Methods

This study uses column O₃ data derived from Nimbus 7 (January 1979 through April 1993) and Earth Probe (EP) (July 1996 through August 1998) TOMS backscattered ultraviolet measurements. TCO and stratospheric column ozone (SCO) in the tropics were obtained from TOMS data using the CCD method [*Ziemke et al.*, 1998]. In the general CCD method, total (i.e., stratospheric plus tropospheric) column O₃ is derived from low-reflectivity ($R < 0.2$) measurements, and stratospheric column O₃ follows from nearby column O₃ measurements taken above the tops of very high tropopause-level clouds with high reflectivity ($R > 0.9$). Reflectivity R in TOMS data is computed using ultraviolet (UV) wavelengths 380 nm for Nimbus 7 and 360 nm for EP TOMS. Because the TOMS instrument measures UV wavelengths, it cannot detect O₃ below cloud tops and must place a predetermined best guess column amount of O₃ below cloud tops. Typical below-cloud column amounts for $R < 0.2$ footprint scenes are at most ~1-2 DU in the version 7 algorithm for either Nimbus 7 or EP TOMS.

To derive CCD TCO in the tropics, SCO is calculated in the Pacific region where tropopause-level clouds are persistent. SCO is derived for every 5° latitude band over longitudes from 120°E eastward to 120°W. These values are then assumed to be independent of longitude in a given latitude band. This assumption is based on the zonal characteristics of tropical SCO as inferred from Upper Atmosphere Research Satellite (UARS) microwave limb sounder (MLS) and halogen occultation experiment (HALOE) data [*Ziemke et al.*, 1998]. With the averaging invoked over the Pacific there is a sufficiently large number of both $R < 0.2$ and $R > 0.9$ footprint measurements to enable the construction of complete monthly time series of tropical TCO. The number of $R > 0.9$ ozone measurements was indicated by *Ziemke et al.* [1998] to average around 300-400 per month for 5° latitude bands from 120°E eastward to 120°W. Compared to $R > 0.9$, the number of $R < 0.2$ footprints significantly exceed $R > 0.9$ and all other reflectivity scenes in the tropical Pacific. In conjunc-

Table 1. Annual Mean Fraction of $R < 0.2$ Footprints in Percent

Latitude	1981	1983	1985	1987	1989	1991
10°N-15°N	73(13)	77(13)	71(12)	75(12)	74(11)	70(14)
5°N-10°N	62(14)	68(16)	62(13)	64(13)	64(13)	60(13)
0°N-5°N	72(12)	72(14)	75(12)	67(13)	76(11)	69(11)
0°S-5°S	76(12)	69(15)	79(11)	72(13)	80(10)	75(11)
5°S-10°S	71(13)	65(15)	74(11)	71(12)	76(11)	73(12)
10°S-15°S	74(14)	74(12)	74(12)	75(12)	77(11)	74(12)

Numbers in parentheses denote one standard deviation in percent. Longitudes are 120°E-240°E.

tion with the averaging done in the Pacific for the CCD method, Table 1 shows the fraction (in percent) of Nimbus 7 $R < 0.2$ ozone footprint scenes averaged from 120°E eastward to 120°W within 5° latitude bands. For a typical year not affected by strong El Niño, the smallest fraction of $R < 0.2$ measurements occurs in the Northern Hemisphere (NH) following the Intertropical Convergence Zone (ITCZ). This is seen in Table 1 for the years 1981, 1985, and 1989, where the smallest fractions (62%-64%) lie in the 5°N-10°N latitude band. In

1983 which was an intense El Niño year, the smallest fraction of $R < 0.2$ footprints instead appears in the 5°S-10°S band.

Measurement uncertainties in TCO from the CCD method are discussed in detail by Ziemke *et al.* [1998]. The largest uncertainties are anticipated to lie in the Atlantic region where the assumption of a zonally invariant stratospheric O₃ column could produce additional errors of several DU in TCO. For all TCO time series shown in this study, 2σ measurement uncertainty

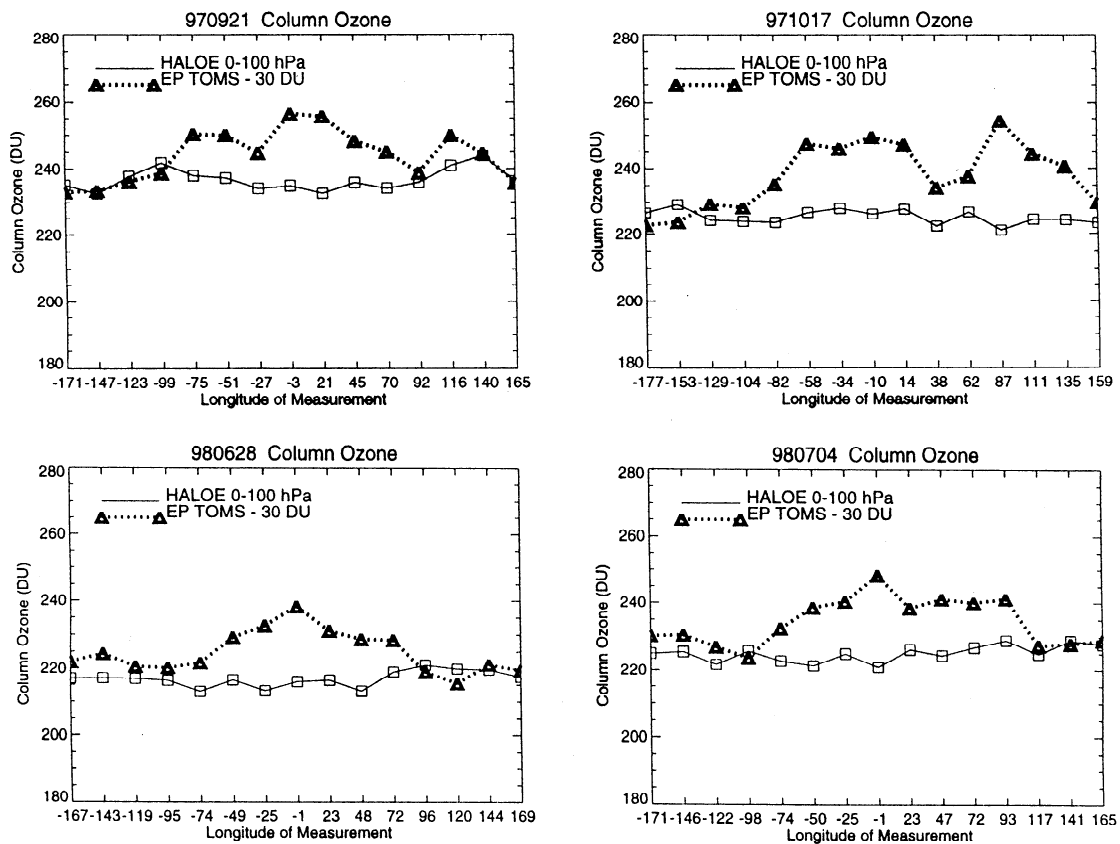


Figure 1. Column ozone (Dobson units) plotted versus longitude for Earth Probe TOMS (dotted) and 0-100 hPa UARS HALOE (solid) during El Niño (top frames, September 21, 1997 and October 17, 1997) and non-El Niño (bottom frames, June 28, 1998 and July 4, 1998) conditions. Earth Probe TOMS total column values were derived from the averaging of four-point nearest neighbor $1^\circ \times 1.25^\circ$ gridded level-3 data coincident with HALOE latitude-longitude locations. (Latitudes for HALOE lie between 10°S and 10°N.) For Earth Probe TOMS total column ozone, 30 Dobson units were subtracted to better visually compare with HALOE column amounts.

errors are estimated to vary approximately uniformly from about 3 DU in the Pacific region up to ~5 DU in the Atlantic.

Examples showing the property of zonal homogeneity of tropical SCO are given in Figure 1, which plots zonal distributions of daily 0-100 hPa SCO derived from HALOE (solid) and colocated EP TOMS total ozone (dashed) for four selected days during and after the recent 1997-1998 El Niño event. Even in daily measurements, the approximation of zonal invariance of SCO appears to be qualitatively valid despite robust changes occurring in tropical convection in the Pacific between El Niño year (top two frames) and non-El Niño

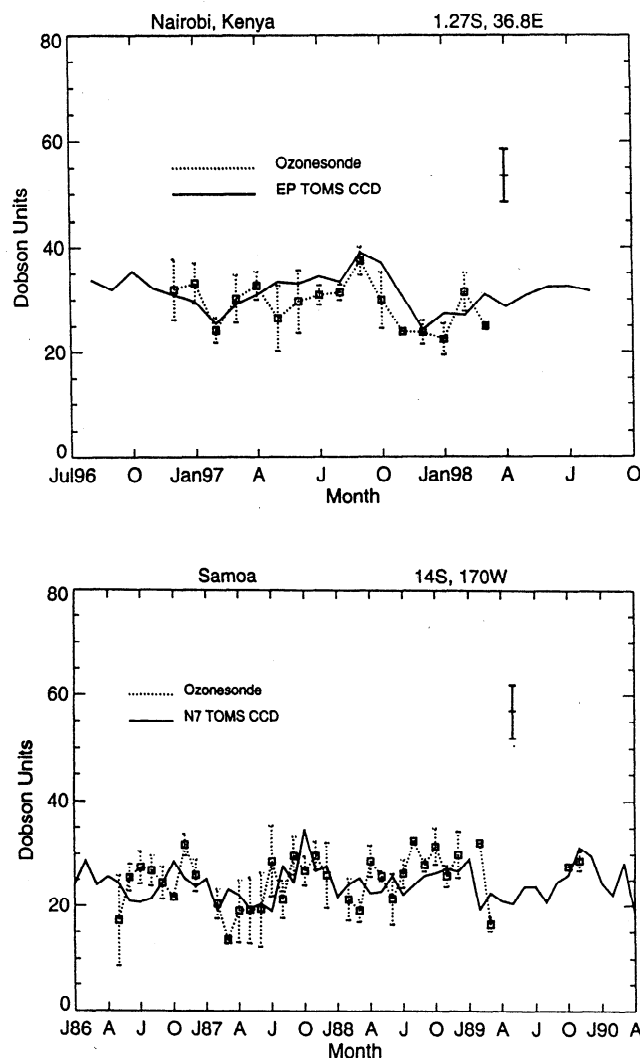


Figure 2. Monthly mean tropospheric column O_3 time series from the CCD method (solid) plotted with coincident ground-based ozonesonde measurements (dotted) at Samoa (14°S , 170°W) and Nairobi (1°S , 37°E). The CCD time at Nairobi used EP TOMS measurements and had 5 DU subtracted relative to Nimbus 7 to account for instrumental bias (discussed in section 3). Uncertainty bars for sonde measurements represent $\pm 1\sigma$ temporal standard deviations. Measurement uncertainty bars for the CCD measurements (upper right in each frame) represent $\pm 2\sigma$ standard deviations.

year (bottom two frames). As shown by Ziemke *et al.* [1998], TCO derived from the CCD method agrees well with available ground-based measurements in the tropics. For example, Figure 2 (not included in Ziemke *et al.* [1998]) shows good qualitative agreement between CCD and ozonesonde TCO time series at both Pacific Samoa (14°S , 170°W) and Nairobi (-1°S , 37°E) in east Africa.

A potential source of error in assuming zonal symmetry of tropical SCO is the temporal and spatial changes in tropopause height. As shown by Logan [1999] and also from our own analyses of tropical sonde data, zonal variability of the tropical tropopause is generally only a few hundred meters, equivalent to (at most) ~ 5 -10 hPa change in tropopause pressure. According to Gage and Reid [1987], seasonal variability of the tropopause height in the tropical Pacific (the region where CCD SCO data are derived) is generally around 1 km (~ 10 hPa tropopause change) with interannual variability smaller at around a few hundred meters. Table 2 shows seasonally averaged tropopause pressures, tropopause heights, TCO, and total number of profiles from tropical stations Ascension Island, Natal, Brazzaville, and Samoa. For clarity, mean standard deviations are not included in Table 2. (Standard deviations can be shown to vary for all these tropical stations by ~ 4 -8 hPa for seasonal tropopause pressures, a few hundred meters for tropopause heights, and ~ 2 -4 DU for TCO). Ozonesonde profiles at Ascension Island and Brazzaville are from 1990-1992, while data from Samoa encompass 1984-1989 and 1995-1996 time periods. The longest and most continuous sonde record is at Natal and spans 1979-1992. Results from Table 2 indicate nearly uniform tropopause pressures (~ 100 hPa) and tropopause heights (~ 17 km) year round in the tropics. As shown by Ziemke and Chandra [1998] and as inferred from Table 2, fluctuations (up to 10 hPa, or 1 km) of the tropopause in the Pacific at Samoa produce at most around 2 DU change in TCO. We also note that TCO amounts given in Table 2 corroborate the existence of the persistent tropical zonal wave 1 distribution [e.g., Fishman and Larsen, 1987; Ziemke *et al.*, 1996; Hudson and Thompson, 1998] with high values in the Atlantic and low values in the Pacific.

3. Three Tropical Regions With Distinctly Different Characteristics

The variability of TCO in the tropics can be generalized by simply examining TCO time series from three different regions that exhibit distinctly different behavior. Figure 3 shows TCO monthly mean time series (dark curves) evaluated along the equator in the eastern Pacific (left), Atlantic (middle), and western Pacific (right) for January 1979-December 1992. Also shown are regression model fits (light curves, discussed below) incorporated to help quantify the different mechanisms

Table 2. Seasonally Averaged Tropopause Pressure P , Tropopause Height H , Tropospheric Column Ozone O_3 , and Number of Profiles N Derived From Available 1978-1996 Tropical Ozonsonde Measurements

Station	Dec.-Feb.				March-May				June-Aug.				Sept.-Nov.			
	P	H	O_3	N	P	H	O_3	N	P	H	O_3	N	P	H	O_3	N
	hPa	km	DU		hPa	km	DU		hPa	km	DU		hPa	km	DU	
Ascension (8°S, 15°W)	91	17.4	41	(17)	95	17.0	31	(16)	106	16.4	45	(7)	95	17.1	46	(26)
Natal (5°S, 35°W)	94	16.9	36	(46)	95	16.9	27	(48)	104	16.4	37	(54)	102	16.5	43	(85)
Brazzaville (4°S, 15°E)	104	16.5	41	(14)	104	16.4	34	(11)	93	17.1	41	(22)	102	16.6	43	(34)
Samoa (14°S, 170°W)	92	17.2	24	(30)	94	17.2	21	(31)	98	16.8	25	(45)	100	16.8	27	(51)

Total number of profiles averaged per season are shown in parentheses.

likely responsible for monthly to decadal variations. For plotting, all time series in Figure 3 were smoothed with a 3-month running average. The time series in this analysis included only data from Nimbus 7 TOMS. Data from EP TOMS, which became available in late July 1996, indicate a persistent and uniform offset of around +5 DU relative to Nimbus 7 in derived TCO in the tropics. Because of this potential bias, TCO from EP TOMS cannot be easily combined with data from Nimbus 7 TOMS in regression analyses. In this study, 5 DU was subtracted from the EP TOMS TCO database. This subtraction of a constant number does not alter the relative variabilities present in the data. We note that the study by Lambert *et al.* [1999] compared EP TOMS total column ozone overpass data with Systeme d'Analyse par Observations Zenithales (SAOZ) total ozone measurements in the tropics, indicating a possible positive offset (based on SAOZ data at Kiribati (1°N, 173°E)) of a few percent in EP TOMS total column ozone. Interestingly, that study also indicated a positive offset in all southern latitudes (based on five SAOZ and two Dobson stations) that was largest for low-reflectivity scenes.

The cause of this potential offset in EP TOMS TCO data is not currently understood but is being investigated. It is not caused by instrument calibration because the CCD method (unlike all other TCO schemes) subtracts two measurements from the same instrument to derive TCO (i.e., TOMS total column O_3 minus TOMS SCO). From our preliminary investigation, the explanation appears to be a subtle secondary effect involving the TOMS algorithm/instrument and low-reflectivity scenes.

The linear regression model used in this study, similar to those described by Stolarski *et al.* [1991], Randel and Cobb [1994], and Ziemke *et al.* [1997], is as follows:

$$TCO(t) = \alpha(t) + \beta(t) t + \gamma(t) QBO(t) + \delta(t) \text{ solar}(t) + \epsilon(t) \text{ ENSO}(t) + R(t). \quad (1)$$

In (1), t represents the month index ($t=1,2,\dots,168$, corresponding to January 1979 through December 1992), and $\alpha, \beta, \gamma, \delta$, and ϵ are time-dependent regression coefficients given (at most) by a constant plus 12-month, 6-month, and 4-month cosine and sine harmonic series. The seasonal-cycle coefficient α was modeled by the seven-term expansion $c_0 + \sum_{j=1}^3 [c_j \cos(2\pi jt/12) + s_j \sin(2\pi jt/12)]$, where c_j and s_j are constants. Each of the other coefficients in (1) were all modeled using a smaller five-term harmonic expansion given by $c_0 + \sum_{j=1}^2 [c_j \cos(2\pi jt/12) + s_j \sin(2\pi jt/12)]$. The error in (1) is the residual series $R(t)$, and the decadal linear trend is given by the coefficient β . Solar(t) in (1) represents the solar proxy (10.7-cm solar flux series), and ENSO(t) is given by the Tahiti minus Darwin sea level pressure time series. QBO(t) in (1) represents the quasi-biennial oscillation (QBO) proxy derived from Singapore (1°N, 140°E) zonal winds using the empirical orthogonal function (EOF) approach of Randel *et al.* [1995] (described previously by Wallace *et al.* [1993]). For TCO a 3-month lag was applied to QBO(t); this time lag was found to provide maximum anticorrelation between TCO and SCO in the tropics, a scenario indicating a possible UV modulation effect on tropospheric O_3 photochemistry caused by QBO-induced changes in SCO. This 3-month lag is comparable to e-folding decay timescales for O_3 in the upper troposphere [e.g., Jacob *et al.*, 1996]. Error analysis for the regression coefficients involved a multivariate method with an additional modulation of coefficient errors using the seasonal cycles present in residual time series. This multivariate approach showed nearly identical monthly coefficient critical values and critical regions when tested against the more extensive Monte Carlo results of Ziemke *et al.* [1997] that included additional errors (~ 2 -5%) for all proxy terms in (1).

Because the focus of our study is the characterization of seasonal and interannual changes in tropical TCO, we do not discuss in detail the solar cycle and linear trend terms in (1). We instead refer the reader to the previous study by Chandra *et al.* [1999] regarding decadal vari-

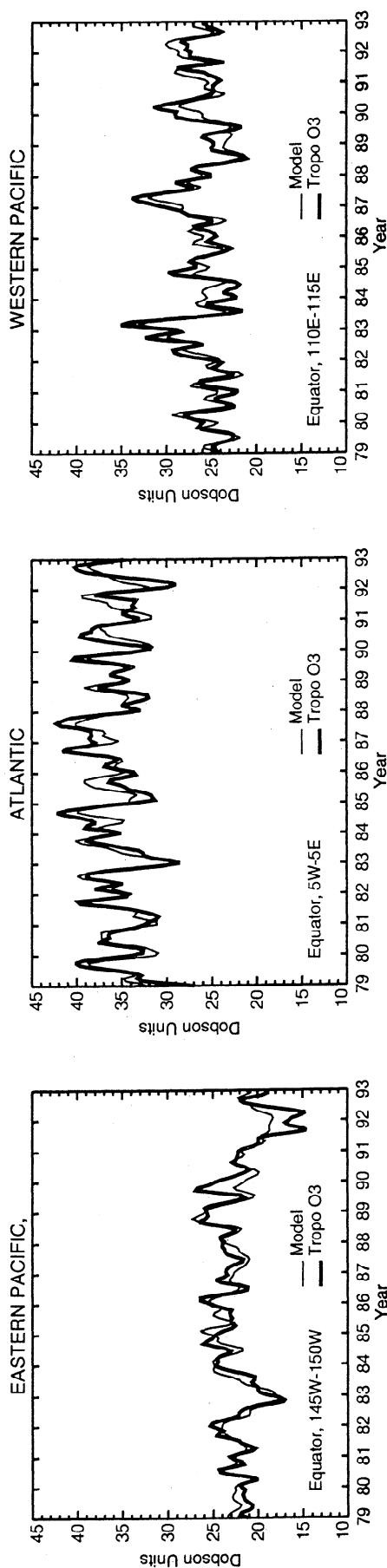


Figure 3. Tropospheric column O_3 time series along the CCD data (heavy) and regression model (light, see section 2). (left) Equator, $145^{\circ}W$ - $150^{\circ}W$ in the eastern Pacific. (middle) Equator, $5^{\circ}W$ - $5^{\circ}E$ in the central Atlantic. (right) Equator, $110^{\circ}E$ - $115^{\circ}E$ in the western Pacific. All time series were derived by averaging data at $2.5^{\circ}S$ and $2.5^{\circ}N$ and include a 3-month running average for plotting. Mean RMS differences between CCD and model time series for these three locations are 2.5, 3.4, and 2.3 DU, respectively.

abilities in tropical TCO which showed a statistically significant solar cycle (anticorrelated with F10.7) and essentially zero trends in the tropics. Chandra *et al.* [1999] indicated that the solar signal in TCO (~ 2 -3 DU peak-to-peak) could not be explained from photochemistry alone and is possibly related to subtle changes in transport over a solar cycle.

Figure 3 indicates consistently high values in the Atlantic compared to the Pacific, where even minimum values of TCO in the Atlantic region are generally greater than the largest values in the Pacific. This identifies what several previous studies have referred to as a primarily zonal wavenumber 1 pattern in tropical TCO first identified by Fishman and Larsen [1987].

Table 3 shows the variances explained by each of the regression terms in (1) for the three time series plotted in Figure 3. These results indicate that the dominant variability (~ 40 -50%) in the Pacific is interannual and appears to be related to El Niño and La Niña events, whereas in the Atlantic the leading source is the annual cycle that explains $\sim 50\%$ of total variance. In the Atlantic there is also evidence of an interannual variability ($\sim 9\%$) associated with the QBO. In the following sections we will attempt to quantify these detected variabilities in TCO beginning with the annual cycle.

4. Annual Cycles

Figure 4 shows 1979-1992 mean annual cycles ($\alpha(t)$ in (1)) for six northern hemisphere (NH) and southern hemisphere (SH) gridpoints coinciding with the same three longitudes in Figure 3. As Ziemke *et al.* [1998] showed, and as also seen in Figure 4, TCO in the SH is largest around SH springtime. Seasonal variability and TCO amount are both smallest in the SH western Pacific. Figure 4 indicates that NH TCO maximizes around NH springtime in both the eastern and western Pacific and in autumn in the central Atlantic. A remarkable result from Figure 4 is a large difference between hemispheres in the seasonal variability of SCO. SCO in the NH shows a large annual cycle change (~ 30 DU peak-to-peak), implying that seasonal variability in total column ozone in the NH tropics is driven mostly by changes in stratospheric O_3 . In comparison, seasonal variability in SH total column O_3 appears largely driven by tropospheric O_3 .

Ziemke *et al.* [1998] previously compared CCD and ozonesonde TCO measurements at Samoa, Natal, Brazzaville, and Ascension Island in the SH tropics. Unfortunately, extensive comparisons are not possible in the NH tropics because of lack of sufficient ozonesonde data. Although located at a more northerly latitude, Hilo ($20^{\circ}N$, $155^{\circ}W$) is one station that has enough sonde data to derive a seasonal climatology for TCO. Despite a reduced number of high-reflectivity cloud scenes at $20^{\circ}N$ compared to the lower latitudes, the CCD method

Table 3. Variance Explained by Individual Terms in (1)

Location	$\Omega(t)$	$\alpha(t)$	βt	γ QBO(t)	δ solar(t)	ϵ ENSO(t)	R(t)
Equator, 112.5°E	7.53(100)	1.92(25.5)	0.31(4.10)	0.16(2.06)	0.15(2.00)	3.04(40.4)	2.48(32.9)
Equator, 0°E	9.41(100)	4.10(46.8)	0.20(2.08)	0.82(8.75)	0.56(5.99)	0.68(7.23)	3.43(36.4)
Equator, 147.5°W	6.33(100)	0.32(4.98)	0.22(3.40)	0.27(4.21)	0.78(12.3)	3.05(48.2)	2.25(35.6)

Values in parentheses are in units of percent of total variance. All other values are in DU².

still yields enough data to provide a seasonal climatology of TCO for comparison. These two climatologies are plotted together in Figure 5. Both time series show a similar seasonal cycle with largest values in spring. The model results of Wang *et al.* [1998b] indicated that this springtime maxima observed at nearby Mauna Loa Observatory could be explained mostly from the transport of pollution from Asia.

Figure 6 shows horizontal cross sections of annual means and annual amplitudes in TCO derived from $\alpha(t)$ in (1). In Figure 6 (top), the largest TCO values greater than 36 DU occur in the south Atlantic, with the smallest values (less than 22 DU) in the Pacific near the dateline. Mean amplitudes of the annual component (Figure 6, bottom) indicate values up to 7 DU over eastern Brazil and 5-6 DU over southern Africa. The 5-7 DU annual amplitudes (i.e., 10-15 DU peak-to-peak seasonal changes) in Figure 6 (bottom) over these regions provide a mean upper bound to seasonal variability in TCO.

Some of the features in the seasonal cycles observed in this study are well simulated in the 3-D photochemical transport model results of Hauglustaine *et al.* [1998] and Wang *et al.* [1998b]. We note that these models included many sources of O₃ production such as biomass burning, burning of fossil fuels, lightning, and soil emissions. In the next section we examine interannual variabilities of TCO in the tropical Atlantic and Pacific regions and establish plausible explanations for those changes.

5. Interannual Variability

A new and important result from this study is the characterization of interannual variabilities in tropical TCO. The comparison of interannual variabilities present in TCO and other geophysical parameters offers insight that cannot be gained by examining only seasonal cycles.

Interannual variabilities in TCO associated with both QBO and ENSO are shown in Figure 7. Given are annual averages of γ and ϵ from (1) with shading indicating regions where these coefficients are not different from zero at the 2 σ level. Figure 7 (top) plots the QBO coefficients which appear statistically significant in the Atlantic region. The signature for ENSO (Figure 7, bottom) shows a dipole pattern centered just west of

the dateline. We note that this Pacific dipole pattern and inflection region for ENSO near 165°-170°E is also present in similar 1979-1992 regression analyses of both NOAA OLR and Goddard GEOS-1 surface temperature data (figures not shown).

Amplitudes (in DU) in TCO attributed to QBO and ENSO can be estimated by multiplying the mean coefficient values in Figure 7 with QBO(t) and ENSO(t) used in (1). Given ± 35 m s⁻¹ extremes present in the EOF QBO wind time series QBO(t), coefficient values of -0.3 to -0.4 seen in Figure 7 (top) in the Atlantic region translate to ~ 2 -3 DU peak-to-peak changes in TCO. (For comparison, we note that the QBO variability in SCO was shown by Ziemke *et al.* [1998] to be ~ 15 -20 DU peak-to-peak.) For ENSO, TCO changes during an El Niño or La Niña event are comparable but slightly larger in amount than QBO. Given 2 hPa extremes present in time series ENSO(t) during either an El Niño or La Niña event, coefficient amplitudes of around 1.5 to 2.0 seen in Figure 7 (bottom) in the western and eastern Pacific region translate to ~ 3 -4 DU anomalies in TCO.

Figure 7 indicates that while interannual variability in the Pacific is dominated by ENSO, variability in the Atlantic region appears to be associated instead with the QBO. The negative sign of $\gamma(t)$ suggests that the QBO in TCO is out of phase with the QBO in SCO with a 3-month phase lag. This is readily seen in Figure 8, which compares the interannual changes in SCO and TCO at 2.5°S centered around 0° longitude (region of largest QBO signal in TCO seen in Figure 7). The time series in Figure 8 were deseasonalized and extended through August 1998 to include more recent EP TOMS data. For EP TOMS TCO, 5 DU column amount was subtracted to account for the possible bias (discussed in section 3). In addition, the TCO time series was lagged by 3 months for maximum anticorrelation with SCO (also discussed in section 3).

Figure 8 suggests an out of phase relationship between SCO and TCO on a QBO timescale over most of 1979-1998 except for a short duration from 1989 to 1991. The out of phase relation suggests that interannual changes in tropospheric O₃ in the tropical Atlantic region may be controlled by photochemical processes which are influenced by the UV flux entering the troposphere. The latter is inversely proportional to stratospheric O₃ which is modulated by the QBO. The

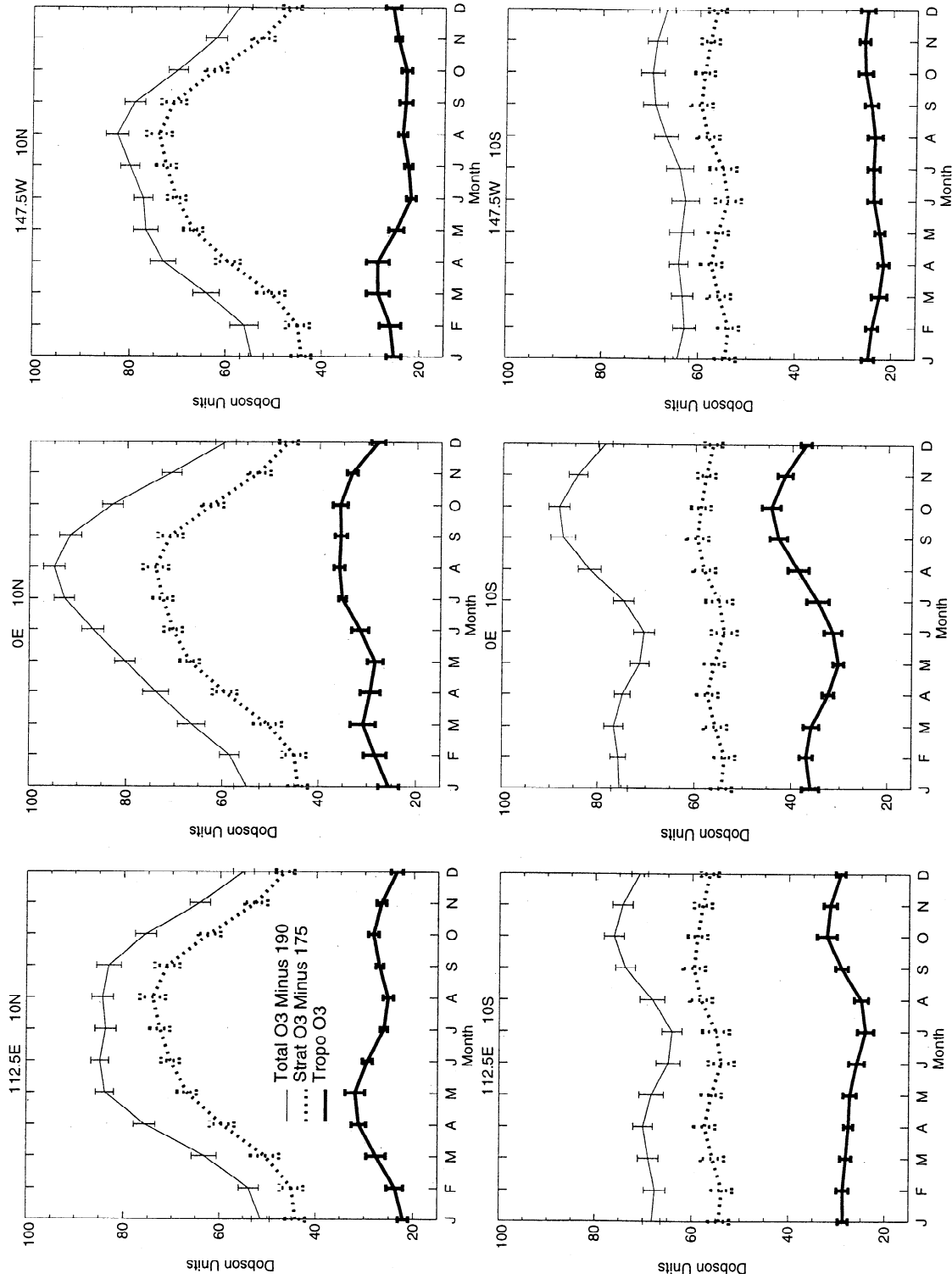


Figure 4. Seasonal cycles $\alpha(t)$ in column O₃ derived from the regression model (see section 2) for total column O₃ (light solid), stratospheric column O₃ (dotted), and tropospheric column O₃ (heavy solid) at six tropical locations (indicated). For better visual comparison with tropospheric column O₃ results, 190 DU (175 DU) was subtracted from total column O₃ (stratospheric column O₃).

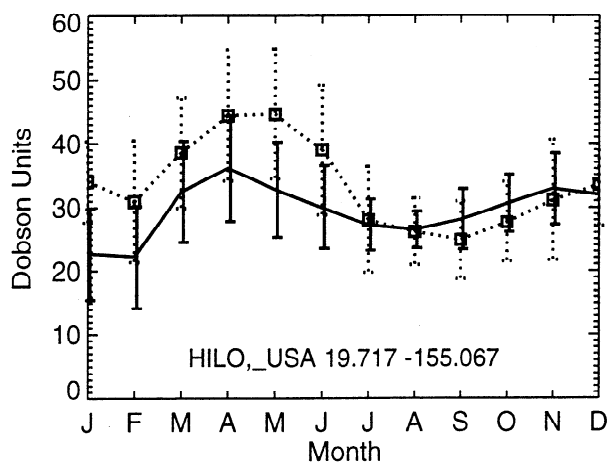


Figure 5. Mean seasonal cycles (in Dobson units) in TCO at Hilo (20°N, 155°W) for ozonesonde (dotted) and CCD (solid) measurements. Sonde and CCD TCO climatologies were derived using all available data between 1982 and 1992. The sonde data included 375 ozone and temperature profiles. Vertical bars represent $\pm 1\sigma$ temporal standard deviations.

3-month phase shift is characteristic of a photochemical time constant for O_3 in the upper troposphere. A UV modulation of upper tropospheric photochemistry in the Atlantic seems to be consistent with a polluted environment compared to the Pacific region. However, even with the higher values of NO_x observed in this region, the UV modulation effect on tropospheric O_3 is generally weak and difficult to explain quantitatively [Chandra *et al.*, 1999].

Another source of interannual variability in TCO in the tropical Atlantic region may be the ozone precursors (CO , NO_x , hydrocarbons) produced by biomass burning. Our study suggests that this is probably a weak source as indicated in Figure 9, which compares TCO and ASI time series in the tropical Atlantic region. The source for the ASI variability is primarily smoke particles lying above the boundary layer ($\sim 1-2$ km altitude) generated by biomass burning. As shown by Herman *et al.* [1997] from Nimbus 7 TOMS ASI data, most aerosols detected by TOMS south of the equator in the Atlantic will be smoke particles rather than dust. In the SH, intense biomass burning over Africa and South America begins around June-July and extends through perhaps October. Dust in northern Africa from the Sahara and Sahel desert regions (spanning latitudes 10°N to 28°N) remains primarily north of the equator for any given month, drifting westward across the Atlantic toward Central and North America. Figure 9 suggests a generally good positive correlative relationship between ASI and TCO for the years 1985 through 1990. However, the behavior between TCO and ASI for the entire period of observation (1979-1998) is not well correlated. A similar conclusion can be shown between TCO and OLR data (figure not shown), indicating that local changes in convection also have a relatively weak impact in interannual changes in TCO. It is possible that the QBO signal observed in TCO in the Atlantic may have a dynamical origin unrelated to ENSO or these other factors.

In contrast to the Atlantic, both the eastern and western Pacific regions are strongly influenced by tropical

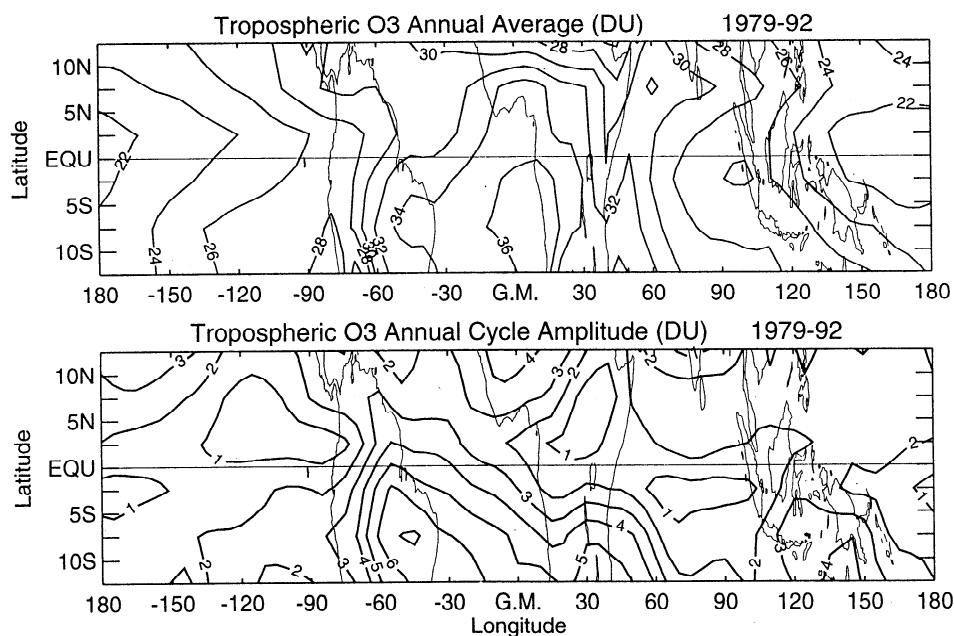


Figure 6. Latitude versus longitude annual means (top) and annual amplitudes (bottom) of 1979-1992 CCD TCO derived from $\alpha(t)$ in (1). Column amounts are in Dobson units.

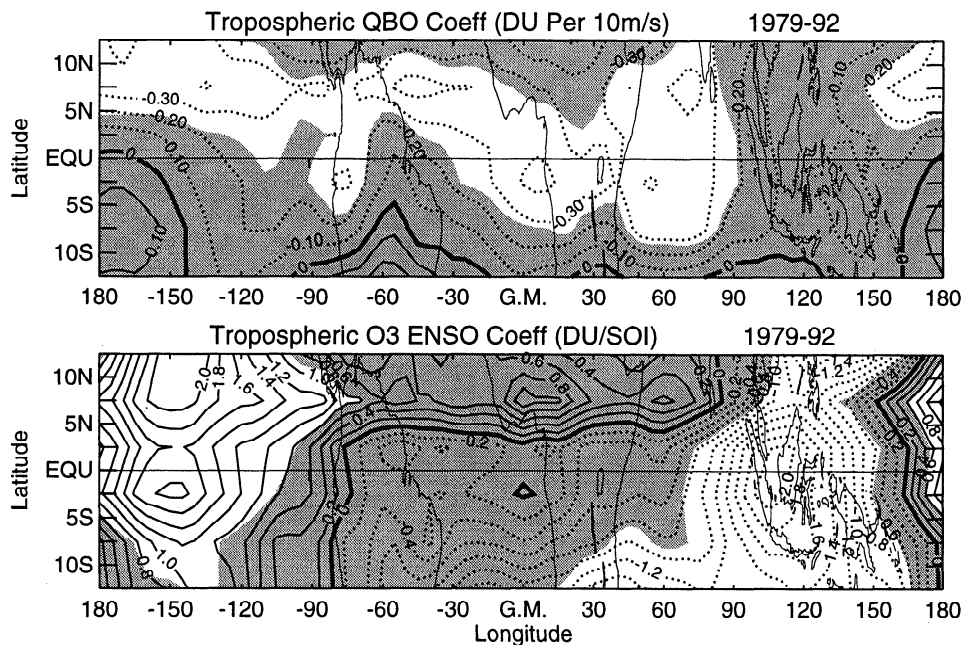


Figure 7. Latitude versus longitude tropospheric column O_3 QBO coefficients (top, in Dobson units per 10 m s^{-1}) and ENSO coefficients (bottom, in Dobson units per unit of $ENSO(t)$) for the same regression model as in Figure 6. Shading indicates regions where coefficients are not different from zero at the 2σ level.

convection as seen earlier in Figure 7 (lower panel) and as further illustrated in Figure 10. Figure 10 shows deseasonalized time series of TCO along the equator in the western Pacific (top) and eastern Pacific (bottom). TCO derived from EP TOMS measurements again includes a subtraction of 5 DU with respect to Nimbus 7. There is evidence of an interannual signal in the eastern and western Pacific associated with the 1982-1983, 1987, 1991-1992, and 1997-1998 El Niño events. Recovery of the 1997-1998 El Niño in TCO and OLR is seen near the end of the record shown, around the months of May and June 1998. Months following June

1998 indicate a shift toward a La Niña condition with a larger than average amount of convection in the western Pacific region.

The observed positive anomalies in TCO in the western Pacific during El Niño in Figure 10 are consistent with suppressed convection and less reduction of TCO from vertically transported low boundary layer O_3 and O_3 -destroying agents (including H_2O), while negative anomalies in the eastern Pacific are consistent with enhanced convection and opposite effects as discussed by Chandra *et al.* [1998]. As indicated by Hauglustaine *et al.* [1998], low O_3 over the Pacific coincides with

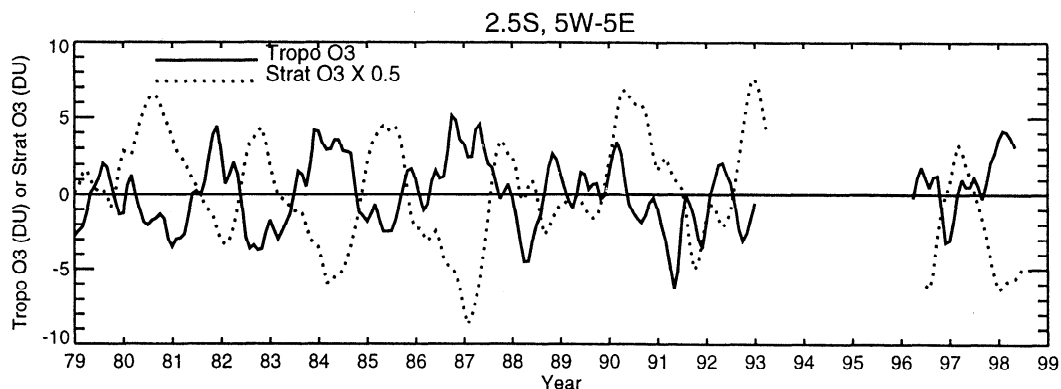


Figure 8. Time series of CCD monthly mean tropospheric column O_3 (solid) plotted versus stratospheric column O_3 (dotted) at 2.5°S averaged between 5°W and 5°E . Stratospheric column O_3 was multiplied by the factor 0.5. The tropospheric column O_3 time series was shifted 3 months backward in time for maximum anticorrelation with stratospheric column O_3 (discussed in section 3). A 3-month running average was applied to both time series for plotting.

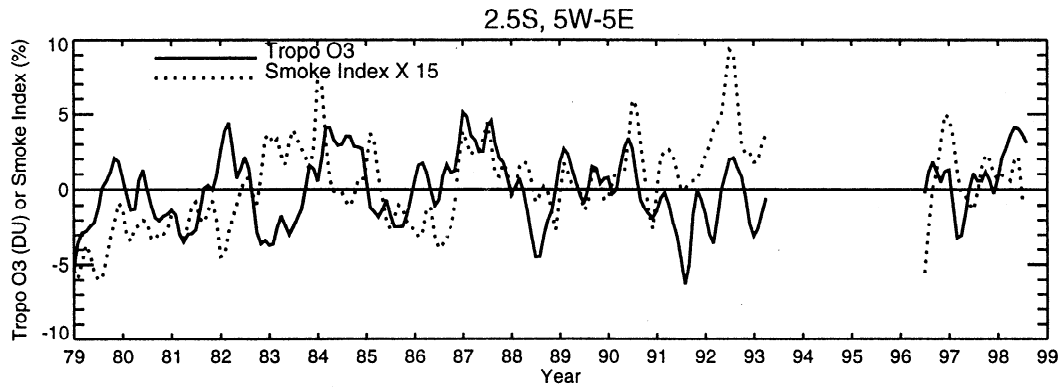


Figure 9. Time series of CCD monthly mean tropospheric column O₃ (solid) plotted with TOMS aerosol-smoke index data (dashed). Aerosol index time series have been rescaled (indicated) for plotting. Both time series include a 3-month running average for plotting.

the rising branch of the Walker circulation and is efficiently transported upward from the marine boundary layer to the upper troposphere. (This is consistent with low O₃ observed in the upper troposphere by *Kley et al.* [1996]).

Plate 1 compares tropical TCO between October 1996 (top) and October 1997 (bottom). The October 1996 plot indicates a normal non-El Niño condition with largest TCO in the Atlantic and lowest TCO in the western Pacific. In October 1997 this pattern changed

dramatically during El Niño, with smallest TCO in the eastern Pacific and largest TCO in the western Pacific over Indonesia. The sizeable ~40-45 DU values of TCO observed over Indonesia in October 1997 are similar to typical amounts present in the tropical Atlantic, which is an oceanic region with biomass burning effects and suppressed convection (including considerable subsidence of air mass) year round.

One can attempt a comparison of the relative impact of convection effects versus biomass burning in

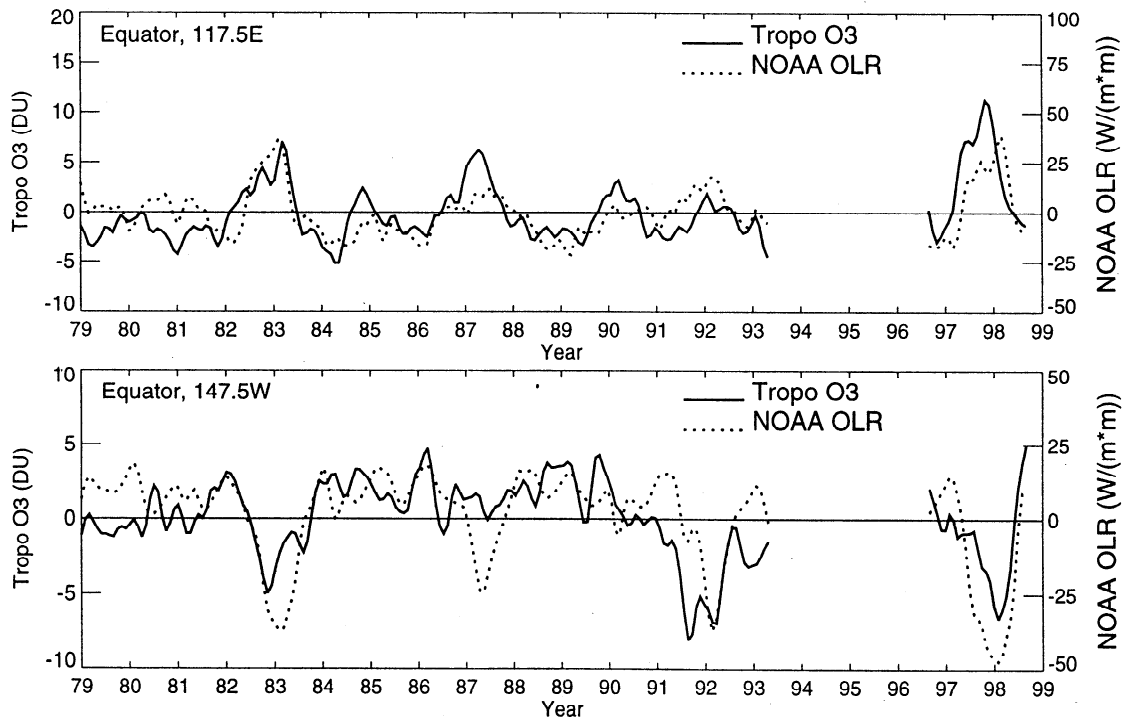


Figure 10. (top) Time series of CCD monthly mean tropospheric column O₃ (solid) plotted versus concurrent NOAA OLR (dotted) along the equator in the western Pacific at longitude 117.5°E. (bottom) Time series of CCD monthly mean tropospheric column O₃ (solid) plotted versus concurrent NOAA OLR (dotted) along the equator in the eastern Pacific at longitude 147.5°W. All time series include a 3-month running average for plotting.

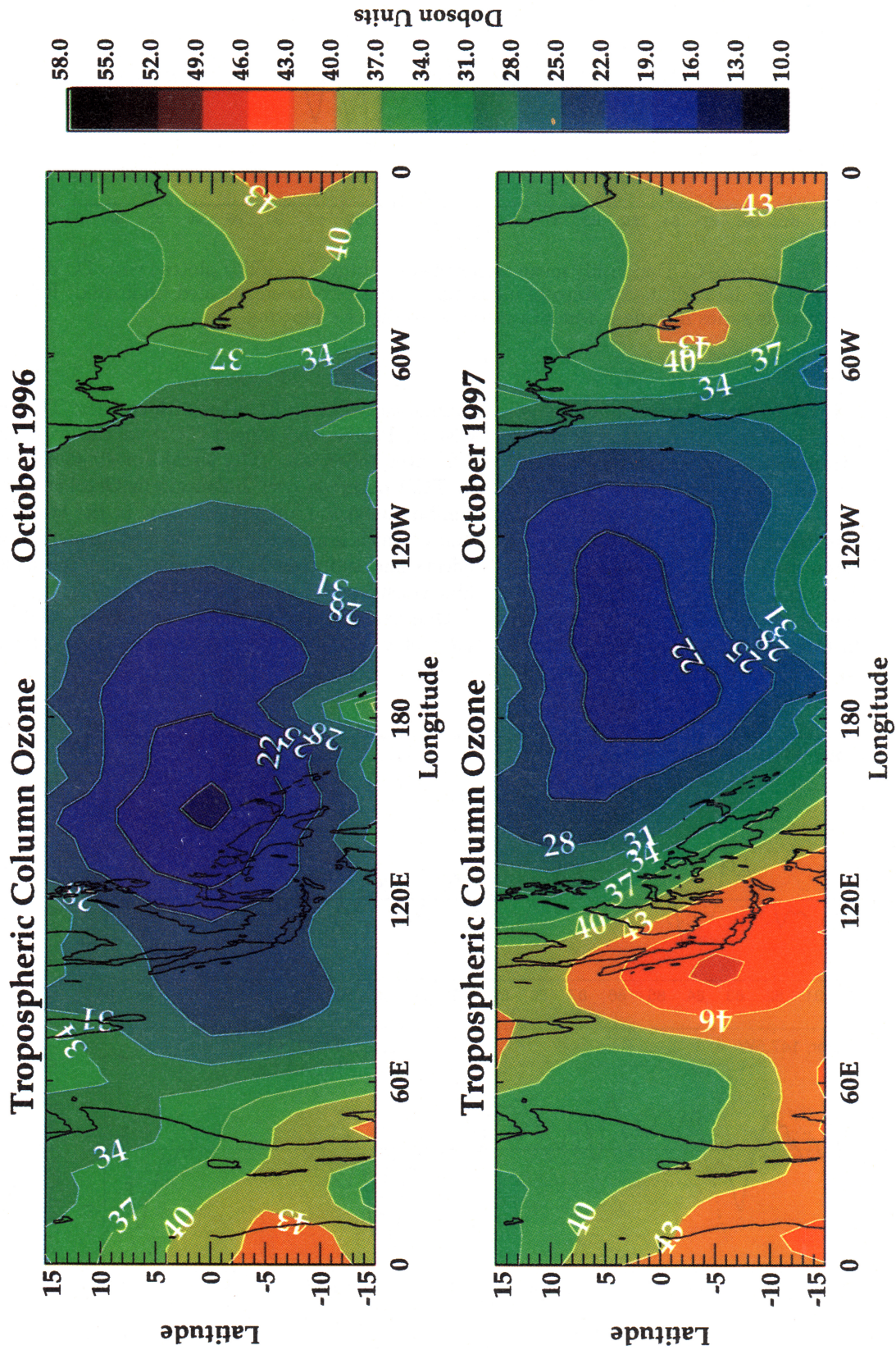


Plate 1. Tropospheric column ozone (Dobson units) in the tropics derived from the CCD method (top) October 1996 and (bottom) October 1997.

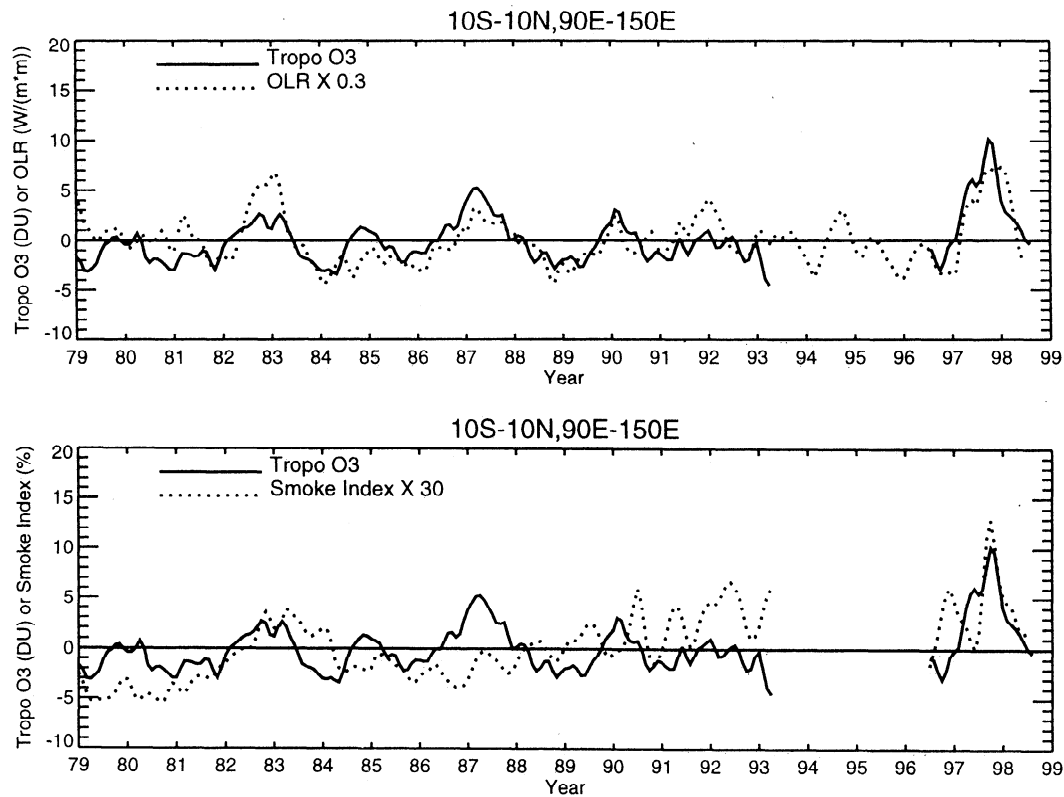


Figure 11. (top) Time series of CCD monthly mean tropospheric column O_3 (solid) plotted versus concurrent NOAA OLR (dotted) averaged over 10°S - 10°N and 90°E - 150°E . (bottom) The same time series of CCD monthly mean tropospheric column O_3 (solid) plotted versus concurrent TOMS aerosol-smoke index data (dotted). Both OLR and aerosol index time series have been rescaled (indicated) in each case. All time series include a 3-month running average for plotting.

the western Pacific region by examining coincident measurements of both NOAA OLR and TOMS ASI. Figure 11 compares time series of deseasonalized TCO, OLR, and ASI averaged over the western Pacific from January 1979 through August 1998. Again, 5 DU was subtracted from original TCO data from EP TOMS relative to Nimbus 7. Although TCO and OLR (Figure 11, top) are coherent over this long time record, the same can be said for TCO and ASI (Figure 11, bottom) particularly during the 1982-1983, 1991-1992, and 1997-1998 El Niño events. It is not possible to distinguish from Figure 11 whether dynamical transport and induced changes in O_3 photochemistry dominate generation of TCO over that of biomass burning during El Niño events because OLR and ASI anomalies are by nature generally positively correlated in this region. During El Niño, OLR in the western Pacific is large because of suppressed convection, and the ensuing dryness results in increased amounts of uncontrolled wildfires and high ASI.

The intense biomass burning over the western Pacific during El Niño events likely generates a considerable amount of O_3 precursors but may be limited to the lower troposphere because of suppressed convection

present over this broad region. Independent of biomass burning, a change in convection in the tropical western Pacific can alter in situ O_3 photochemistry in the troposphere. Conceivably, suppressed convection during El Niño in the western Pacific oceanic region results in an increase in TCO because of reduced transport of both low-value boundary layer O_3 and O_3 -destroying agents (including H_2O), and the downward motion of O_3 -producing air mass in the middle and upper troposphere [Chandra *et al.*, 1998]. It would be a useful effort (beyond the scope of this study) to try to reproduce these interannual variabilities detected in tropical TCO using 3-D photochemical transport models.

6. A Simplified Method for Deriving Tropical Tropospheric Column Ozone

An important result from this study was identifying the western Pacific near the dateline as a region with small seasonal variability (see Figure 6) and little or no ENSO or QBO interannual signals in TCO (see Figure 7). Because of small variability of TCO in this region, a simplified method is proposed to estimate the tropical TCO distribution from only total column ozone gridded

measurements. This technique is discussed in detail in the appendix. We call this the simplified tropospheric ozone residual (STOR) method, to distinguish it from the CCD method. The direct CCD method in comparison requires high-resolution footprint measurements of reflectivity and total ozone, and also the presence of tropopause-level clouds.

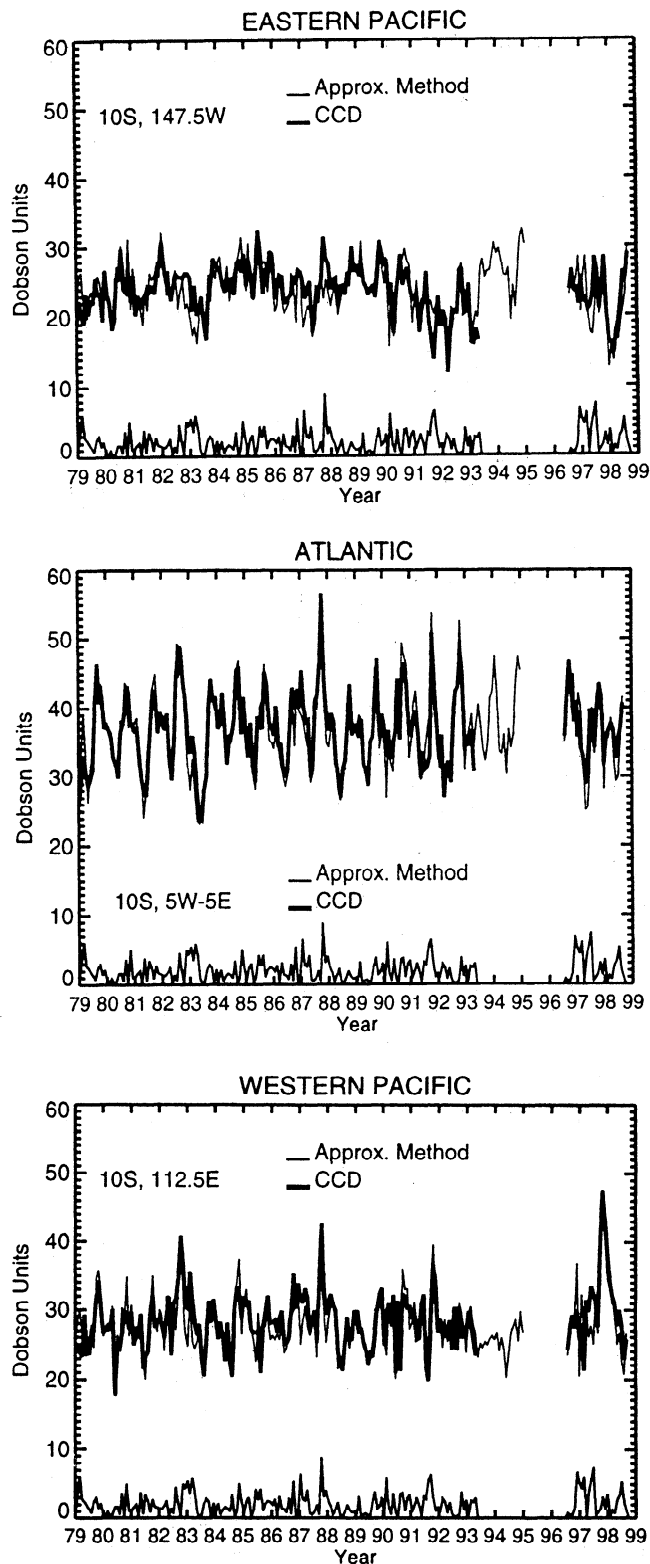


Figure 12 compares 1979-1998 TCO time series between the CCD and simplified method at 10°S in the eastern Pacific, Atlantic, and western Pacific regions. Also included in these time series are NOAA 11 solar backscatter ultraviolet/2 (SBUV2) total column O₃ measurements for May 1993 through November 1994 to help bridge the gap of missing data between the Nimbus 7 and EP TOMS time periods. Absolute value differences are plotted along the bottom of each frame. Despite simplicity of the STOR technique, Figure 12 shows good agreement with CCD measurements (mean absolute differences ~2-4 DU).

The STOR method is primarily useful for studying interannual and shorter timescales and can produce higher horizontal resolution than the 5° × 5° gridding used in this investigation. This method can be easily applied to SBUV and BUV total column ozone measurements to help fill the gap between Nimbus 7 and EP TOMS time periods and to provide a merged (30+ years) TCO database extending backward in time to April 1970 (the beginning of the 1970-1977 BUV total ozone data set).

7. Summary

The variability of O₃ in the tropical troposphere can be generalized by simply examining time series from three different regions: the western Pacific, the central Atlantic, and the eastern Pacific. Away from the Atlantic region, seasonal variability in NH tropical TCO derived from the CCD method indicates maximum amounts around NH spring months; in contrast, the greatest amounts in SH TCO occur around SH spring months. Throughout the central Atlantic there was shown to be a dominant annual cycle with maximum TCO around SH spring. An interesting result was that seasonal variability in NH total column O₃ appears dominated by seasonal changes in stratospheric O₃, in contrast to the SH in which seasonal cycles are driven

Figure 12. Tropospheric column O₃ time series at 10°S from the CCD method (heavy) and simplified method (light; see appendix): (left) 10°S, 145°W-150°W in the eastern Pacific, (middle) 10° S, 5°W-5°E in the central Atlantic, (right) 10°S, 110°E-115°E in the western Pacific. These time series along 10°S were generated by averaging data at 12.5°S and 7.5°S. The simplified method includes total ozone data from NOAA SBUV2 for May 1993-December 1994 to help fill in data between the demise of Nimbus 7 TOMS and the beginning of Earth Probe TOMS. Plotted along the bottom of each frame are absolute value differences between CCD and the simplified method. The 1979-1998 mean RMS difference between CCD and the simplified method is 2.7 DU for these data at 10°S. Mean RMS differences for data at original latitudes 12.5°S, 7.5°S, 2.5°S, 2.5°N, 7.5°N, and 12.5°N are 3.8, 3.6, 3.3, 2.9, 3.6, and 3.6 DU, respectively.

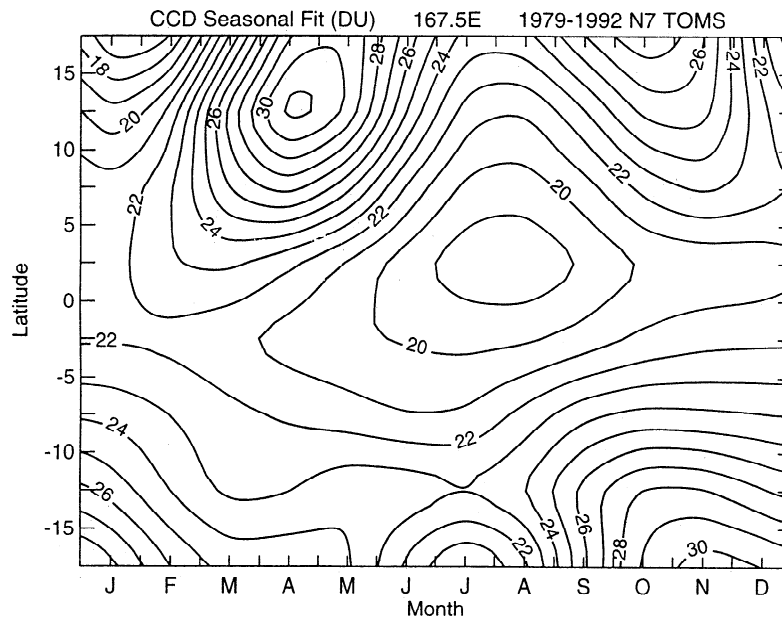


Figure 13. Nimbus 7 TOMS 1979-1992 CCD seasonal fit $\alpha(t)$ (in Dobson units) along longitude 167.5°E (see section 2). Contour interval is 1 Dobson unit.

largely by tropospheric O_3 . These regional differences in TCO seasonal-cycles were validated from ozonesonde data in this study and from results of previous investigations.

A new result from this study was a characterization of interannual variabilities in tropical TCO. By comparing interannual variabilities in TCO and other geophysical parameters (e.g., OLR, ASI), we have gained a better insight of this relationship than by examining only seasonal cycles. Previous studies have established a strong link between biomass burning and tropospheric O_3 in the tropical Atlantic based on the seasonal characteristics of TCO. Our study finds that interannual variability of TCO in the Atlantic exhibits a QBO-varying signal that is out of phase with the QBO present in SCO. The QBO in TCO in this region represent changes (peak-to-peak) of around 2-3 DU compared to around 15-20 DU in SCO. This QBO behavior in TCO seems to be consistent with UV modulation of upper tropospheric

photochemistry on a QBO timescale caused by the QBO in stratospheric ozone. However, photochemical models tend to underpredict these changes in TCO. The interannual variability seen in TCO in the Atlantic appears to have influence from biomass burning, but this may have a lesser impact. It is also possible that dynamics is a critical factor in producing the detected QBO in TCO.

Examination of TCO time series in the Pacific indicates that during El Niño events there exists low values of TCO in the eastern Pacific and high values in the western Pacific. These anomalies represent around 3-4 DU interannual changes in TCO. This behavior is consistent with enhanced and suppressed convection effects in the eastern and western Pacific region, respectively, as discussed by *Chandra et al.* [1999]. Interannual variabilities in these regions appear to be associated with convectively driven upward transport of low-value boundary layer O_3 (reducing TCO) and O_3 -destroying

Table 4. CCD 1979-1992 Seasonal Fit Tropospheric Column O_3 at 167.5°E

Latitude	Jan.	Feb.	March	April	May	June	July	Aug.	Sept.	Oct.	Nov.	Dec.
17.5°	16.7	17.4	22.7	28.4	30.0	27.3	23.8	23.5	26.1	28.0	26.1	20.9
12.5°	19.9	21.7	26.9	31.2	30.9	26.2	21.2	20.0	22.6	25.6	25.3	22.2
7.5°	21.6	23.0	25.7	27.3	25.9	22.3	19.2	18.7	20.6	22.8	23.2	22.2
2.5°	21.7	22.6	23.1	22.4	20.8	19.0	18.1	18.1	18.9	19.7	20.2	20.8
-2.5°	22.1	21.7	21.0	20.3	19.9	19.7	19.8	20.0	20.3	20.9	21.5	22.0
-7.5°	23.8	22.6	21.8	21.6	21.7	21.7	21.6	21.9	22.7	24.0	24.9	24.8
-12.5°	25.6	23.2	22.3	23.0	23.9	24.1	23.7	24.0	25.7	27.9	29.1	28.1
-17.5°	27.5	25.1	24.9	25.5	24.6	21.8	19.5	20.4	24.8	29.9	32.4	31.0

Values are in Dobson units.

Table 5. CCD 1979-1992 Seasonal Fit Tropospheric Column O₃ 2 σ at 167.5°E

Latitude	Jan.	Feb.	March	April	May	June	July	Aug.	Sept.	Oct.	Nov.	Dec.
17.5°	3.4	4.4	4.6	5.4	3.4	2.5	1.8	1.2	1.3	1.6	2.3	3.7
12.5°	2.6	3.1	2.9	2.5	2.0	1.4	1.1	1.0	1.3	1.6	1.7	2.0
7.5°	1.2	2.2	1.4	1.6	1.6	1.1	0.9	0.9	1.1	1.5	1.1	1.6
2.5°	0.8	1.3	1.4	1.5	1.3	0.7	0.7	1.3	1.6	1.1	1.2	0.9
-2.5°	1.1	1.7	1.3	1.4	0.9	0.8	0.9	1.5	1.7	0.9	1.6	1.0
-7.5°	1.2	1.5	1.7	1.0	1.4	1.0	1.2	1.4	1.4	1.8	1.9	1.2
-12.5°	0.8	1.0	1.4	1.1	1.1	1.5	1.3	2.4	1.7	2.5	2.1	1.8
-17.5°	1.3	1.4	1.7	1.2	2.0	2.2	2.2	4.2	3.0	2.7	2.1	2.0

Values are in Dobson units.

precursors. Low boundary layer O₃ over the Pacific occurs in the rising branch of the Walker circulation and is transported upward to the upper troposphere. The observed increase of 10-20 DU in TCO in the western Pacific during the recent 1997-1998 El Niño appears to be a manifestation of reduced convection (which changes the photochemistry of O₃ in the troposphere) and ozone generated from biomass burning.

Lastly, a simplified technique (denoted STOR) is introduced in this study for deriving maps of TCO in the tropics. This promising approach requires only total column O₃ gridded measurements and utilizes the small variability in TCO near the dateline. Monthly mean TCO computed from this technique was shown to differ on average (over 1979-1998) by only 2-4 DU from direct CCD-derived TCO. This simplified technique compliments the CCD method in the absence of high-reflecting clouds and is useful for studying interannual and shorter timescales and also smaller horizontal scales than the 5° × 5° gridding used in this study. In addition, the STOR approach can be applied to SBUV and BUUV total column O₃ measurements to help fill the temporal gap between Nimbus 7 and EP TOMS and also to extend the analysis of TCO backward in time to include the 1970-1977 BUUV time period.

Appendix: Simplified Tropospheric Ozone Residual Method

The simplified tropospheric ozone residual (STOR) method makes use of weak interannual variability in TCO at a chosen reference longitude near the dateline. This reference longitude is chosen to be 167.5°E, which lies near the center of the observed inflection region in ENSO variability (see Figure 7, bottom). We note that the QBO-related variability in this region (Figure 7, top) is also small (~1 DU). With these assumptions, TCO in (1) can be represented by only the seasonal component $\alpha(t)$ provided that the solar cycle and linear trend terms can also be neglected. As shown by Chandra *et al.* [1999], linear trends in TCO are not statistically significant anywhere in the low-latitude tropics, with small changes of at most ~1 DU per decade.

In addition, changes in TCO related to the solar cycle were shown to be about 2-3 DU and may also be neglected for studying interannual and shorter timescales. In the STOR method, SCO is first derived at the reference longitude λ_0 by subtracting $\alpha(t)$ in (1) from total column ozone Ω :

$$SCO(\lambda_0, \phi, t) = \Omega(\lambda_0, \phi, t) - \alpha(\lambda_0, \phi, t). \quad (A1)$$

In (A1), λ is the longitude (λ_0 is reference longitude), ϕ is latitude, and t represents the month.

We next assume to first approximation (as with the CCD method) that *SCO* is zonally invariant and hence the same at all longitudes λ . Tropospheric column O₃ (*TCO*) at each grid point is then derived by subtracting zonally invariant *SCO* in (A1) from coinciding gridded measurements of $\Omega(\lambda, \phi, t)$:

$$TCO(\lambda, \phi, t) = \Omega(\lambda, \phi, t) - \Omega(\lambda_0, \phi, t) + \alpha(\lambda_0, \phi, t). \quad (A2)$$

Figure 13 shows values of $\alpha(t)$ at reference longitude 167.5°E, with meridional coverage extended to ±17.5°. Tables 4 and 5 list the values plotted in Figure 13 and their 2 σ uncertainties. Hence, given only total ozone gridded measurements in the tropics, TCO can be estimated by simply combining (A2) with the values shown in Table 4 for $\alpha(t)$. Values in Table 4 may be interpolated to generate ozone maps for time averages shorter than 1 month used in this study.

In conclusion, we mention that differences between TCO derived from the CCD and STOR approaches are independent of longitude. This follows because stratospheric column amounts for both methods are assumed to be zonally invariant. The absolute-value differences plotted in Figure 12 for 10°S must therefore be equivalent for all three time series shown.

Acknowledgments. We greatly appreciate the efforts of members of NOAA and of the UARS and TOMS data processing teams in producing the extensive geophysical data sets used in this study. We are particularly grateful to Omar Torres, Christina Hsu, and Jay Herman for helpful discussions regarding the aerosol-smoke index data used in this study. We also wish to thank P. K. Bhartia and the two anonymous reviewers for important comments and suggestions regarding this paper.

References

- Brasseur, G. P., J. T. Kiehl, J.-F. Müller, T. Schneider, C. Granier, X. Tie, and D. Hauglustaine, Past and future changes in global tropospheric ozone: Impact on radiative forcing, *Geophys. Res. Lett.*, *25*, 3807-3810, 1998.
- Chandra, S., J. R. Ziemke, W. Min, and W. G. Read, Effects of 1997-1998 El Niño on tropospheric ozone and water vapor, *Geophys. Res. Lett.*, *25*, 3867-3870, 1998.
- Chandra S., J. R. Ziemke, and R. W. Stewart, An 11-year solar cycle in tropospheric ozone from TOMS measurements, *Geophys. Res. Lett.*, *26*, 185-188, 1999.
- Crutzen, P. J., and M. O. Andreae, Biomass burning in the tropics: Impact on atmospheric chemistry and biogeochemical cycle, *Science*, *250*, 1669-1678, 1990.
- Fishman, J., and J. C. Larsen, Distribution of total ozone and stratospheric ozone in the tropics: Implications for the distribution of tropospheric ozone, *J. Geophys. Res.*, *92*, 6627-6634, 1987.
- Fishman, J., C. E. Watson, J. C. Larsen, and J. A. Logan, Distribution of tropospheric ozone determined from satellite data, *J. Geophys. Res.*, *95*, 3599-3617, 1990.
- Fishman, J., K. Fakhruzzaman, B. Cros, and D. Nganga, Identification of widespread pollution in the southern hemisphere deduced from satellite analyses, *Science*, *252*, 1693-1696, 1991.
- Fishman, J., V. G. Brackett, and K. Fakhruzzaman, Distribution of tropospheric ozone in the tropics from satellite and ozonesonde measurements, *J. Atmos. Terr. Phys.*, *54*, 589-597, 1992.
- Fishman, J., V. G. Brackett, E. V. Browell, and W. B. Grant, Tropospheric ozone derived from TOMS/SBUV measurements during TRACE A, *J. Geophys. Res.*, *101*, 24,069-24,082, 1996.
- Fuglestedt, J. S., J. E. Johnson, and I. S. A. Isaksen, Effects of reductions in stratospheric ozone on tropospheric chemistry through changes in photolysis rates, *Tellus, Ser. B*, *46*, 172-192, 1994.
- Gage, K. S., and G. C. Reid, Longitudinal variations in tropical tropopause properties in relation to tropical convection and El Niño-Southern Oscillation events, *J. Geophys. Res.*, *92*, 14,197-14,203, 1987.
- Haigh, J. D., The impact of solar variability on climate, *Science*, *272*, 981-984, 1996.
- Hauglustaine, D. A., G. P. Brasseur, S. Walters, P. J. Rasch, J.-F. Müller, L. K. Emmons, and M. A. Carroll, MOZART, a global chemical transport model for ozone and related chemical tracers, 2, Model results and evaluation, *J. Geophys. Res.*, *103*, 28,291-28,335, 1998.
- Herman, J. R., P. K. Bhartia, O. Torres, N. C. Hsu, C. J. Seftor, and E. Celerier, Global distribution of absorbing aerosols from Nimbus-7/TOMS data, *J. Geophys. Res.*, *102*, 16,911-16,922, 1997.
- Hsu, N. C., J. R. Herman, P. K. Bhartia, C. J. Seftor, O. Torres, A. M. Thompson, J. F. Gleason, T. F. Eck, and B. N. Holben, Detection of biomass burning smoke from TOMS measurements, *Geophys. Res. Lett.*, *23*, 745-748, 1996.
- Hudson, R. D., and A. M. Thompson, Tropical tropospheric ozone (TTO) from TOMS by a modified-residual method, *J. Geophys. Res.*, *103*, 22,129-22,145, 1998.
- Jacob, J., et al., Origin of ozone and NO_x in the tropical troposphere: A photochemical analysis of aircraft observations over the South Atlantic basin, *J. Geophys. Res.*, *101*, 24,235-24,250, 1996.
- Kley, D., P. J. Crutzen, H. G. J. Smit, H. Vomel, S. J. Oltmans, H. Grassi, and V. Ramanathan, Observations of near-zero ozone concentrations over the convective Pacific: Effects on air chemistry, *Science*, *274*, 230-232, 1996.
- Krishnamurti, T. N., H. E. Fuelberg, M. C. Sinha, D. Oosterhof, E. L. Bensen, and V. B. Kumar, The meteorological environment of the tropospheric ozone maximum over the tropical South Atlantic Ocean, *J. Geophys. Res.*, *98*, 10,621-10,641, 1993.
- Krishnamurti, T. N., M. C. Sinha, M. Kanamitsu, D. Oosterhof, H. Fuelberg, R. Chatfield, D. J. Jacob, and J. Logan, Passive tracer transports relevant to the TRACE A Experiment, *J. Geophys. Res.*, *101*, 23,889-23,907, 1996.
- Lambert, J.-C., M. V. Roozendael, M. D. Maziere, P. C. Simon, J.-P. Pommereau, F. Goutail, A. Sarkissian, and J. F. Gleason, Investigation of pole-to-pole performances of spaceborne atmospheric chemistry sensors with the NDSC, *J. Atmos. Sci.*, *56*, 176-193, 1999.
- Liebmann, B., and C. A. Smith, Description of a complete (interpolated) outgoing longwave radiation dataset, *Bull. Am. Meteorol. Soc.*, *77*, 1275-1277, 1996.
- Liu, S. C., and M. Trainer, Responses of the tropospheric ozone and odd hydrogen radicals to column ozone change, *J. Atmos. Chem.*, *6*, 221-233, 1988.
- Logan, J. A., An analysis of ozonesonde data for the troposphere: Recommendations for testing 3-D models, and development of a gridded climatology for tropospheric ozone, *J. Geophys. Res.*, in press, 1999.
- Madronich, S., The atmosphere and UV-B radiation at ground level, in *Environmental UV Photobiology*, edited by A. R. Young et al., pp. 1-39, Plenum, New York, 1993.
- Randel, W. J., and J. B. Cobb, Coherent variations of monthly mean total ozone and lower stratospheric temperature, *J. Geophys. Res.*, *99*, 5433-5447, 1994.
- Randel, W. J., F. Wu, J. M. Russell III, J. W. Waters, and L. Froidevaux, Ozone and temperature changes in the stratosphere following the eruption of Mount Pinatubo, *J. Geophys. Res.*, *100*, 16,753-16,764, 1995.
- Stolarski, R. S., P. Bloomfield, R. D. McPeters, and J. R. Herman, Total ozone trends deduced from Nimbus 7 TOMS data, *Geophys. Res. Lett.*, *18*, 1015-1018, 1991.
- Thompson, A. M., K. E. Pickering, D. P. McNamara, M. R. Schoeberl, R. D. Hudson, J. H. Kim, E. V. Browell, V. W. J. H. Kirchhoff, and D. Nganga, Where did tropospheric ozone over southern Africa and the tropical Atlantic come from in October 1992? Insights from TOMS, GTE/TRACE-A and SAFARI-92, *J. Geophys. Res.*, *101*, 24,251-24,278, 1996.
- Wallace, J. M., R. L. Panetta, and J. Estberg, Representation of the equatorial stratospheric quasi-biennial oscillation in EOF phase space, *J. Atmos. Sci.*, *50*, 1751-1762, 1993.
- Wang, Y., D. J. Jacob, and J. A. Logan, Global simulation of tropospheric O₃ - NO_x-hydrocarbon chemistry, 1, Model formulation, *J. Geophys. Res.*, *103*, 10,713-10,726, 1998a.
- Wang, Y., D. J. Jacob, and J. A. Logan, Global simulation of tropospheric O₃ - NO_x-hydrocarbon chemistry, 3, Origin of tropospheric ozone and effects of nonmethane hydrocarbons, *J. Geophys. Res.*, *103*, 10,757-10,768, 1998b.
- Watson, C. E., J. Fishman, and H. G. Reichle Jr., The significance of biomass burning as a source of carbon monoxide and ozone in the southern hemisphere tropics: A satellite analysis, *J. Geophys. Res.*, *95*, 16,443-16,450, 1990.
- Ziemke, J. R., and S. Chandra, On tropospheric ozone and the tropical wave 1 in total column ozone, in *Proceedings 18th Quadrennial Ozone Symposium, vol. 1*, Parco Scientifico e Tecnologico d'Abruzzo, L'Aquila, Italy, pp. 447-450, 1998.
- Ziemke, J. R., S. Chandra, A. M. Thompson, and D. P. McNamara, Zonal asymmetries in southern hemisphere column ozone: Implications of biomass burning, *J. Geophys. Res.*, *101*, 14,421-14,427, 1996.

Ziemke, J. R., S. Chandra, R. D. McPeters, and P. A. Newman, Dynamical proxies of column ozone with applications to global trend models, *J. Geophys. Res.*, *102*, 6117–6129, 1997.

Ziemke, J. R., S. Chandra, and P. K. Bhartia, Two new methods for deriving tropospheric column ozone from TOMS measurements: The assimilated UARS MLS / HALOE and convective-cloud differential techniques, *J. Geophys. Res.*, *103*, 22,115–22,127, 1998.

S. Chandra, NASA Goddard Space Flight Center, Chemistry and Dynamics Branch, Code 916, Greenbelt, MD 20771. (e-mail: chandra@chapman.gsfc.nasa.gov)

J. R. Ziemke, Software Corporation of America, Beltsville, MD 20705. (e-mail: ziemke@jwocky.gsfc.nasa.gov)

(Received January 22, 1999; revised April 19, 1999; accepted April 30, 1999.)